

Title: Digital holographic microscopy for the evaluation of human sperm structure.

Running title: Human sperm holography

5 **Authors:** Coppola G¹., Di Caprio G²., Wilding M¹., Ferraro P³., Esposito G¹., Di Matteo L¹.,
Dale R¹., Coppola G²., Dale B¹.

Addresses:

10 ⁽¹⁾Centro Fecondazione Assistita (CFA-Italia), Via Manzoni 15, 80123 Naples, Italy; ⁽²⁾Istituto per la
Microelettronica e i Microsistemi, del Consiglio Nazionale delle Ricerche, Sezione di Napoli, Via P.
Castellino, 111, 80131 Naples, Italy; ⁽³⁾Istituto Nazionale di Ottica, del Consiglio Nazionale delle
Ricerche, Sezione di Napoli, c/o Comprensorio Olivetti, Via Campi Flegrei 34 - 80078 Pozzuoli,
Italy.

15

Correspondance: Tel: +39 081641689; Fax: +39 0815479251; e-mail gcoppola@cfa-italia.com

Key words: male infertility, human sperm structure, vacuoles, digital holographic microscopy

20

ABSTRACT

The morphology of the sperm head has often been correlated with the outcome of in vitro fertilization (IVF), and has been shown to be the sole parameter in semen of value in predicting the success of intracytoplasmic sperm injection (ICSI) and intracytoplasmic morphologically selected sperm injection (IMSI).
25

In this paper, we have studied whether Digital Holographic (DH) microscopy may be useful to obtain quantitative data on human sperm head structure and compared this technique to high power digitally enhanced Nomarski microscope. The main advantage of DH is that a high resolution 3-D quantitative sample imaging may be obtained thorough numerical refocusing at different object
30 planes without any mechanical scanning. We show that DH can furnish useful information on the dimensions and structure of human spermatozoo, that cannot be revealed by conventional phase contrast microscopy. In fact, in this paper DH has been used to evaluate volume and indicate precise location of vacuoles, thus suggesting its use as an additional useful prognostic quantitative tool in assisted reproduction technology (ART).

35

INTRODUCTION

Following the advent of human in vitro fertilization (Step toe and Edwards, 1978), much attention has been given to identifying, first embryo morphology, and later, oocyte morphology, as a prognostic tool (Elder and Dale, 2011); less attention has been given to sperm morphology. The spermatozoon delivers the haploid male genome to the oocyte, introduces the centrosome and triggers the oocyte egg into activity.

The sperm head may be considered in three parts; the nucleus with a haploid set of chromosomes, in which deoxyribonucleic acid (DNA) is packaged into a volume that is typically less than 10% of the volume of a somatic cell nucleus (Dadoune, 2003; Elder and Dale, 2011); the acrosome, a large Golgi-derived secretory vesicle on the proximal hemisphere of the head containing an array of hydrolytic enzymes used for digesting the zona pellucida during penetration (Gerton, 2002; Yoshinaga and Toshimori, 2003); and the perinuclear theca, a rigid capsule composed of disulfide bond stabilized structural proteins amalgamated with various other protein molecules (Ok o, 1995).

Human spermatozoa exhibit a wide range of shapes. A number of studies indicate that sperm morphology best predicts the outcome of natural fertilization (Kruger et al., 1988; Bartoov et al., 1999), intra-uterine insemination (Berkovitz et al., 1999) conventional IVF (Kruger et al., 1988; Mashlach et al., 1992) and ICSI (Palermo et al., 1993; Bartoov et al., 2003), and several techniques have been described that provide valuable information on the morphology and pathological features of spermatozoa. In a classical clinical evaluation, human sperm are fixed, stained and analyzed by optical microscopy. Recently, a number of novel techniques have been developed for the identification of more detailed features of cells. Differential interferometric contrast microscopy, scanning near-field optical microscopy, electrostatic force microscopy, atomic force microscopy and scanning thermal microscopy (Bartoov et al., 2002; Akaki et al., 2002; Rothery et al., 2003). Most of these techniques involve biochemical processing that requires specific equipment and may also alter the vitality of the sperm analysed.

The sperm cell is almost transparent in conventional bright field microscopy, since its optical properties differ slightly from the surrounding liquid, generating little contrast. However, a light beam that passes through a spermatozoon undergoes a phase change, in comparison to the surrounding medium, the amplitude of which depends on the light source, the thickness and the integral refractive index of the object itself. A qualitative visualization of this phase contrast may be obtained by contrast interference microscopy (phase contrast or Nomarski/Zernicke interferential contrast microscopy). Recently, efforts have been renewed to improve Differential Interferometric Contrast methods in order to provide quantitative information in microscopy (Kou et al., 2010; Bon et al., 2009). On the other hands over the last few years, DH has been established as a valid non-invasive, quantitative, label free, high resolution, phase-contrast imaging technique in microscopy. In fact, this technique has been successfully applied to image a variety of cell types (Carl et al., 2004; Marquet et al., 2005; Kemper et al., 2006; Charrière et al., 2006; Di Caprio et al., 2010) to obtain additional information about their structure. In a recent preliminary study in human spermatozoa using DH, a statistically significant difference in phase shift was observed when comparing normal sperm with oligoasthenozoospermic sperm (Crha et al., 2011), however the authors did not measure standard morphological parameters using this technique, nor investigate the characteristics of sperm with nuclear vacuoles. One of the main advantages of DH is that a high-resolution 3-D quantitative sample imaging can be automatically produced by numerical refocusing of a 2-D image at different object planes without any mechanical scanning (Dubois et al., 1999; Ferraro et al., 2005). Moreover, using a single acquired image it is possible both to reduce the size of the mass storage devices required for image saving and to achieve a fast image transfer. In this study, we have compared semi-automated digitally enhanced Nomarski microscopy (DESA) with DH to study morphometrical, morphological and volumetrical measurements in normal and vacuolated human spermatozoa. In particular, it is shown that DH is a viable tool for measuring the head volume either in the presence as well as in absence of vacuoles.

MATERIALS AND METHODS

Specimen collection and analytical procedures

Ejaculates were collected by masturbation from 15 males scheduled to undergo IVF at the Centro
90 Fecondazione Assistita (CFA), Naples. After liquefaction, 0.5-1.0 ml of each specimen was
processed using a double-density-gradient centrifugation method (Percoll, Sydney IVF). The final
pellets were resuspended in Ham's F-10 (Gibco) and used to prepare slides for DESA. Briefly, a
semen aliquot containing 2×10^6 spermatozoa was washed 2x by centrifugation with phosphate-
buffered saline (PBS). Then the pellet was suspended in 100 μ l of 2% formaldehyde in PBS and
95 fixed for 10 min at room temperature. A 10 μ l aliquot was then spotted onto a clean microscope
slide, allowed to air dry and mounted with PBS:Glycerol (1:1) (v/v).

In order to compare same cells by both DESA and DH, a grid of 20x20 circles (with a radius of
100 μ m) was placed over the microscope. This grid was made by a photolithographic process that
allows the transfer of the shape of the grid from a mask to a photo-sensitive polymer. At the end of
100 this process, the whole surface of the slide was covered with a 1 μ m-thick photo-sensitive material
except the circles. A 10 μ l aliquot was then spotted on the grid and finally a cover slide was placed
to seal all. Only cells that fell in the circles of the grid were analysed (Fig 1).

Slides were first examined under immersion oil using an inverted microscope (TI-DH; Nikon
Instruments Italia) equipped with Nomarski optics enhanced by digital imaging to achieve a
105 magnification of up to X 1500. The images were captured by a colour video camera for high-quality
image production and analysed using image processing software (NIS-Element Documentation,
Nikon).

Principles of Digital Holography

110 In holography, an object is illuminated by a collimated, monochromatic, coherent light with a
wavelength λ . The object scatters the incoming light forming a complex wavefield (the *object*

beam):

$$O_{x,y} = |O_{x,y}| e^{j\varphi(x,y)} \quad (1)$$

where $|O|$ is the amplitude and φ the phase, x and y denote the Cartesian coordinates in the plane
115 where the wavefield is recorded (*hologram plane*). The phase $\varphi(x,y)$ incorporates information about
the topographic profile of the object under investigation because it is related to the optical path
difference (OPD), which depends on the refractive index and height both of the biological sample
and of the material containing the object itself :

$$\varphi(x,y) = \frac{2\pi}{\lambda} \cdot \text{OPD} \quad (2)$$

120 where a transmission configuration has been considered. The purpose of holography is to capture
the complete wavefront, and in particular the phase φ to obtain quantitative information about the
topographic profile of the object (Cuche et al., 1999). Since all light sensitive sensors respond to
intensity only, the phase is encoded in the intensity fringe pattern adding another coherent
background wave $R(x,y) = |R(x,y)| e^{j\varphi(x,y)}$, called the *reference beam*. This beam and the object
125 beam interfere at the surface of the recording device. The *hologram* is proportional to the intensity
of this interference pattern. In Digital Holography the hologram is acquired by a CCD (or CMOS)
camera array, i.e. a two-dimensional rectangular raster of $M \times N$ pixels, with pixel pitches Δx and
 Δy in the two directions.

130 ***Image reconstruction***

The image reconstruction procedure allows the retrieval of a discrete version of the complex optical
wavefront present on the surface of the object under test. This optical wavefront is obtained by a
numerical back propagation of spatially filtered product between the acquired hologram and a
numerical replica of the reference beam (Cuche et al., 1999; Coppola et al., 2004; Ferraro et al.,
135 2004). Thus, the reconstruction procedure allows to simultaneously determine both the intensity and
especially the phase distribution $\varphi(m,n)$ of the optical wavefront of the specimen. Where $\varphi(m,n)$ is

the discretized version of the phase distribution $\varphi(x,y)$ and m,n are positive integer numbers that identify the m -th row and n -th column of the pixels matrix of the CCD (CMOS) camera. By inverting eq. (2) and considering an homogeneous material with refractive index n_c , from the
140 reconstructed phase distribution, the thickness distribution $s(m,n)$ of the object under investigation can be obtained as follows:

$$OPD_{m,n} = \frac{\lambda}{2\pi} \varphi(m,n) = \frac{\lambda}{2\pi} \arctan \frac{\text{Im}[Q_{m,n}]}{\text{Re}[Q_{m,n}]} \quad (3)$$

where $Q(m,n)$ is the discrete version of the optical reconstructed wavefront on the object surface, Im and Re are the imaginary and real part of the reconstructed optical field, respectively. The relation
145 between the OPD and the thickness of the cell is $OPD(m,n) = s(m,n) \cdot (n_c - n_s)$ where n_c is the refractive index of the cell and n_s is the refractive index of the surrounding medium.

Finally, the possibility offered by Digital Holography to manage the phase of the reconstructed image allows the removal and/or compensation of any unwanted wave front variations, such as optical aberrations (spherical, coma, tilt) and slide deformations (Ferraro et al., 2003; Coppola et al.,
150 2010).

Statistical analysis

Statistical analyses were carried out by Student's t test. Probability values lower than or equal to 0.05 were considered significant.

155 RESULTS

A total of 2000 digitized sperm heads were analysed for six primary parameters (length, width, perimeter, area, number and size of vacuoles). DESA analysis revealed that the mean values for length, width, perimeter and area of the sperm head were $5.18 \pm 0.64\mu\text{m}$ (mean \pm SD) (range: 3.63 to 7.87), $3.53 \pm 0.45\mu\text{m}$ (range: 2.37 to 5.62), $13.75 \pm 1.35\mu\text{m}$ (range: 9.64 to 19.68), $14.12 \pm$
160 $3.03\mu\text{m}^2$ (range: 7.77 to 25.82). In the fifteen ejaculates 62.8% of spermatozoa with one or more vacuoles were found. The number of vacuoles per sperm ranged from 0 to 8 (mean: 2.01 ± 1.78) measuring $0.03\text{-}5.90\mu\text{m}^2$ in area (Fig. 2).

We used DH to evaluate the morphology of 200 of the afore-mentioned spermatozoa (Fig. 3).

Figure 3A is an example of an acquired hologram, with the fringe pattern highlighted in the inset.

165 In Fig. 3B a pseudocolor plot of the phase-contrast map reconstruction of a human spermatozoon is shown. The colour-bar shows the value in rad of the phase difference which depends on the optical density and thickness of the biological sample. Fig. 3C illustrates the quantitative reconstructed morphology obtained by applying eq. 3 to the phase-map contrast.

It is important to note that this three-dimensional image is obtained from the reconstruction of a
170 single acquired hologram, without the use of any mechanical scanning, allowing us to carry out numerical analyses of the six primary sperm parameters mentioned above. No significant differences were observed in the gross morphometric values of the sperm cells analyzed (using DESA or DH; Table 1).

In Fig. 4A and Fig. 4B we show the quantitative profiles of a spermatozoon along the lines AA' and
175 BB' illustrated in Fig.3A, respectively. These profiles show, point by point, a quantitative value of the phase shift due to spermatozoan structure. Quantitative phase shift information from DH allows us to calculate the volume/mass of the sperm head. In Fig. 5, for example, an isoline plot relative to different heights of the sample is displayed. For each region defined by the isolines, the occupied area and the relative volume has been numerically estimated. The analysis revealed that the mean
180 value for volume in normal sperm is $8.03 \pm 0.72\mu\text{m}^3$.

In Fig. 6 we show a quantitative comparison between a control spermatozoon and a spermatozoon with vacuoles. Fig 6A and B illustrates the height profile along the major axis of the sperm head for the defect-free spermatozoon and the spermatozoon with vacuoles, respectively. In Fig. 6E the two profiles are shown together to stress the differences. It's worth to note that both the shapes and the point by point value of the height are different. In particular, the spermatozoon with vacuoles has a distinct depression in the profile (see the arrow in the figure). The profile of the normal spermatozoon results higher than that of the spermatozoon with vacuoles, whereas their 2D dimensions (such as area, and axes length) are similar. The difference in height difference implies a volume difference between the normal spermatozoon and the spermatozoon with vacuoles.

185

190 Table 2 shows three distinct groups of spermatozoa defined using two morphometric variables, head length and head width. The mean values of the volume for the three subpopulations were $5.76 \pm 0.73 \mu\text{m}^3$ (for length $< 2.9 \mu\text{m}$ and width $< 4.2 \mu\text{m}$), $8.24 \pm 0.78 \mu\text{m}^3$ (for $2.9 < \text{length} < 3.7 \mu\text{m}$ and $4.2 < \text{width} < 5.3 \mu\text{m}$), $10.13 \pm 0.81 \mu\text{m}^3$ (for length $> 3.7 \mu\text{m}$ and width $> 5.3 \mu\text{m}$). Mean values of the total volume of the spermatozoa minus the vacuoles volume are also reported.

195 **DISCUSSION**

Here we have used DH as a novel approach for a more advanced morphological analysis of human spermatozoa, in particular to measure the head volume in the presence and absence of vacuoles.

In human sperm, the presence of vacuoles has been related to poor outcome in ART (Berkovitz et al., 2006), an increase in DNA fragmentation (Franco et al., 2008; Wilding et al., 2010) and
200 abnormal chromatin packaging (Franco et al., 2011).

Nuclear vacuoles have been described as a crater defect in the spermatozoa of stallion (Johnson and Hurtgen, 1985), as a pouch formation (Bane and Nicander, 1965), a diadem defect (Blom, 1977) or a nuclear sperm defect (Miller et al., 1982) in bull spermatozoa, and as a crater defect (Johnson and Truitt-Gibert, 1982) or a pouch formation (Bane and Nicander, 1965) in boar spermatozoa. The
205 defect is believed to originate during spermiogenesis as vacuoles have been found in both early and late spermatids (Johnson and Truitt-Gibert 1982). Nuclear vacuoles were shown by electron microscopy to be narrow-mouthed invaginations of the nuclear membrane into the nucleoplasm often filled with an amorphous, cytoplasmic material (Barth 1989). The predominant locations of the vacuoles are the apical region and the acrosome-postacrosomal sheath junction but they have
210 also been found throughout the sperm head (Barth 1989).

Our results show that spermatozoa with vacuoles had a reduced volume probably due to variation of the inner structure of the sperm head with loss of material. We suggest that vacuolated spermatozoa with normal length and width (Bartoov et al., 2002) should be avoided for selection during the ICSI or IMSI procedure, until we acquire more data on the integrity and volume normal viable
215 spermatozoon.

Recently, we have employed a microfluidic-system with DH on unstained bovine spermatozoa in their natural physiological surroundings (Di Caprio et al., 2010). This raises the possibility to use the same technique for a more complete analysis of human spermatozoa, with the additional possibility of sorting cells according to specific morphological criteria.

220 **REFERENCES**

- Akaki, M., Nagayasu, E., Nakano, Y., Aikawa, M., 2002. Surface charge of Plasmodium falciparum merozoites as revealed by atomic force microscopy with surface potential spectroscopy. Parasitol. Res. 88, 16-20.
- 225 Bane, A., Nicander, L., 1965. Pouch formations by invaginations of the nuclear envelope of bovine and porcine sperm as a sign of disturbed spermiogenesis. Nord Vet. Med. 17, 628-632.
- Barth, A.D., 1989. In: Barth, A.D., Oko, R.J., ed. Abnormal Morphology of Bovine Spermatozoa. Iowa State University Press., Ames, IA.
- 230
- Bartoov, B., Eltes, F., Pansky, M., Lederman, H., Caspi, E., Soffer, Y., 1999. Estimating fertility potential via semen analysis data. Hum. Reprod. 8, 65-70.
- Bartoov, B., Berkovitz, A., Eltes, F., Kogosowski, A., Menezes, Y., Barak, Y., 2002. Real-time fine
235 morphology of motile human sperm cells is associated with IVF-ICSI outcome. J. Androl. 23, 1-8.
- Berkovitz, A., Eltes, F., Soffer, Y., Zabludovsky, N., Beyth, Y., Farhi, J., Levran, D., Bartoov B., 1999. ART success and in vivo sperm cell selection depend on the ultramorphological status of spermatozoa. Andrologia. 31, 1-8.
- 240
- Berkovitz, A., Eltes, F., Lederman, H., Peer, S., Ellenbogen, A., Feldberg, B., Bartoov, B., 2006. How to improve IVF-ICSI outcome by sperm selection. Reprod. Biomed. Online. 12, 634-638.
- Blom, E., 1977. Sperm morphology with reference to bull infertility. In: Blom, E., ed. Proc. First
245 All-India Symp. Anim. Reprod., Ludhiana, pp. 61-81.

- Bon, P., Maucort, G., Wattellier, B., Monneret, S., 2009. Quadriwave lateral shearing interferometry for quantitative phase microscopy of living cells. *Opt. Express*. 17, 13080-13094.
- 250 Carl, D., Kemper, B., Wernicke, G., von Bally, G., 2004. Parameter optimized digital holographic microscope for high resolution living cell analysis, *Appl. Opt.* 43, 6536- 6544.
- Charrière, F., Marian, A., Montfort, F., Kuehn, J., Colomb, T., Cuche, E., Marquet, P., Depeursinge, C., 2006. Cell refractive index tomography by digital holographic microscopy”, *Opt. Lett.* 31, 178-
255 180.
- Coppola, G., Ferraro, P., Iodice, M., De Nicola, S., Finizio, A., Grilli, S., 2004. Digital Holographic Microscope for static and dynamic characterization of MEMS. *Meas. Sci. Technol.* 1, 529–539.
- 260 Coppola G., Di Caprio G., Gioffré M., Puglisi R., Balduzzi D., Galli A., Miccio L., Paturzo M., Grilli S., Finizio A., Ferraro P., 2010. Digital self-referencing quantitative phase microscopy by wavefront folding in holographic image reconstruction. *Opt. Lett.* **35**, 3390-3392.
- 265 Crha, I., Zakova, J., Huser, M., Ventruba, P., Lousova, E., Pohanka., M., 2011. Digital holographic microscopy in human sperm imaging. *J. Assist. Reprod. Genet.* 28, 725-729.
- Cuche, E., Marquet, P., Depeursinge, C., 1999. Simultaneous amplitude-contrast and quantitative phase-contrast microscopy by numerical reconstruction of Fresnel off-axis holograms. *Appl. Opt.* 38, 6994-7001.

270

- Dadoune, J.P., 2003. Expression of mammalian spermatozoal nucleoproteins. *Microsc. Res. Tech.* 61, 56–75.
- [Di Caprio, G.](#), [Gioffrè, M.A.](#), [Saffioti, N.A.](#), [Grilli, S.A.](#), [Ferraro, P.A.](#), [Puglisi, R.A.](#), [Balduzzi, D.A.](#), [Galli, A.A.](#), [Coppola, G.](#), 2010. Quantitative label-free animal sperm imaging by means of digital holographic microscopy. *IEEE J. Sel. Top. Quant. Electron.* 16, 833-840
- Dubois, F., Joannes, L., Legros, J.C., 1999. Improved three-dimensional imaging with a digital holographic microscope with a source of partial spatial coherence. *Appl. Opt.* 38, 7085-7094.
- Elder, K., Dale, B., 2011. *In-vitro fertilization*. Cambridge University Press., third ed. pp. 35.
- Ferraro, P., De Nicola, S., Finizio, A., Coppola, G., Grilli, S., Magro, C., Pierattini, G., 2003. Compensation of the inherent wave front curvature in digital holographic coherent microscopy for quantitative phase-contrast imaging. *Appl. Opt.* 42, 1938-1946.
- Ferraro, P., Coppola, G., Alfieri, D., De Nicola, S., Finizio, A., Pierattini, G., 2004. Controlling Images Parameters in the reconstruction process of Digital Holograms. *IEEE JSTQE.* 10, 829-883.
- Ferraro, P., Grilli, S., Alfieri, D., De Nicola, S., Finizio, A., Pierattini, G., Javidi, B., Coppola, G., Striano, V., 2005. Extended focused image in microscopy by digital holography. *Opt. Express.* 13, 6738-6749.
- Franco Jr., JG, Baruffi, RL., Mauri, AL., Petersen, C.G., Oliveira, J.B., Vagnini, L., 2008. Significance of large nuclear vacuoles in human spermatozoa: implications for ICSI. *Reprod. Biomed. Online.* 17, 42-45.

- 300 Franco Jr., J.G., Mauri, A.L., Petersen, C.G., Massaro, F.C., Silva, L.F., Felipe, V., Cavagna, M.,
Pontes, A., Baruffi, R.L., Oliveira, J.B., Vagnini, L.D., 2011. Large nuclear vacuoles are indicative
of abnormal chromatin packaging in human spermatozoa. *Int. J. Androl.* doi: 10.1111/j.1365-
2605.2011.01154.x. [Epub ahead of print]
- Gerton, G., 2002. Function of the sperm acrosome, in: *Fertilization*, ed. D Hardy, San Diego
Academic Press, 265–302.
- 305 Johnson, L.A., Truitt-Gibert , A.J., 1982. Incidence and ultrastructure of abnormalities in porcine
spermatozoa. *Ann. N.Y. Acad. Sci.* 383, 466-468.
- Johnson, L.A., Hurtgen, J.P., 1985. The morphological and unltrastructural appearance of the crater
310 defect in stallion spermatozoa. *Gamete Res.* 12, 41-46.
- Kemper, B.D., Carl Schnekenburger, J., Bredebusch, I., Schäfer, M., Domschke, W., von Bally, G.,
2006. Investigations on living pancreas tumor cells by digital holographic Microscopy. *J. Biomed.*
Opt. 11, 034005.
- 315 Kou, S.S., Waller, L., Barbastathis, G., Sheppard, C.J.R., 2010. Transport-of-intensity approach to
differential interference contrast (TI-DIC) microscopy for quantitative phase imaging. *Opt. Lett.* 35,
447-449.
- 320 Kruger, T.F., Acosta, A.A., Simmons, K.F., Swanson, R.J., Matta, J.F., Oehninger, S., 1988.
Predictive value of abnormal sperm morphology in vitro fertilization. *Fertil. Steril.* 49, 112-117.

- Marquet, P., Rappaz, B., Magistretti, P.J., Cuche, E., Emery, Y., Colomb, T., Depeursinge, C.,
2005. Digital holographic microscopy: a non invasive contrast imaging technique allowing
325 quantitative visualization of living cells with sub wavelength accuracy. *Opt. Lett.* 30, 468 – 470.
- Mashiach, R., Fisch, B., Eltes, F., Tadir, Y., Ovadia, J., Bartoov, B., 1992. The relationship between
sperm ultrastructural features and fertilizing capacity in vitro. *Fertil. Steril.* 57, 1052-1057.
- Miller, D.M., Hrudka, F., Cates, W.F., Mapletoft, R.J., 1982. Infertility in a bull with a nuclear
330 sperm defect: a case report. *Theriogenology* 17, 611-621.
- Oko, R.J., 1995. Developmental expression and possible role of perinuclear theca proteins in
mammalian spermatozoa. *Reprod. Fertil. Dev.* 7, 777–797.
- 335 Palermo, G., Joris, H., Devroey, P., Van Steirteghem, A.C., 1992. Pregnancies after intracytoplasmic
injection of single spermatozoon into an oocyte. *Lancet* 340, 17-18.
- Rothery, AM., Gorelik, J., Bruckbauer, A., Yu, W., Korchev, Y.E., Klenerman, D., 2003 A novel
light source for SICM-SNOM of living cells. *J. Microsc.* 209, 94-101.
340
- Stephoe, P.C., Edwards, R.G., 1978. Birth after the reimplantation of a human embryo. *Lancet.* 12,
366.
- Wilding, M., Coppola, G., Di Matteo L., Palagiano, A., Fusco, E., Dale, B., 2011. Intracytoplasmic
345 injection of morphologically selected spermatozoa (IMSI) improves outcome after assisted
reproduction by deselecting physiologically poor quality spermatozoa. *J. Assist. Reprod. Genet.* 28,
253-262.

World Health Organization. 2010. WHO Laboratory Manual for the Examination and Processing of
350 Human Semen, 5th ed. Geneva.

Yoshinaga, K., Toshimori, K., 2003. Organization and modifications of sperm acrosomal molecules during spermatogenesis and epididymal maturation. *Microsc. Res. Tech.* 61, 39-45.

TABLES

355 Table 1: Mean morphometric values of normal sperm heads obtained by DESA and DHM techniques.

Technique	Length ($\mu\text{m}\pm\text{SD}$)	Width ($\mu\text{m}\pm\text{SD}$)	Perimeter ($\mu\text{m}\pm\text{SD}$)	Area ($\mu\text{m}^2\pm\text{SD}$)	Volume ($\mu\text{m}^3\pm\text{SD}$)
DESA	5.18 \pm 0.64	3.53 \pm 0.45	13.75 \pm 1.35	14.12 \pm 1.95	-
DHM	5.62 \pm 0.31	2.95 \pm 0.51	14.33 \pm 1.22	12.98 \pm 1.25	8.03 \pm 0.75

360

Table 2: Mean volumetric values of vacuolated sperm clustered in three different subpopulations

Sperm dimensions	Volume ($\mu\text{m}^3\pm\text{SD}$)	
	Total	Total - Vacuoles
Length < 2.9 μm Width < 4.2 μm	5.76 \pm 0.73	3.99 \pm 0.76
2.9 < Length < 3.7 μm 4.2 < Width < 5.3 μm	8.24 \pm 0.78	6.40 \pm 0.80
Length > 3.7 μm Width > 5.3 μm	10.13 \pm 0.81	8.42 \pm 0.79

365

370

FIGURE LEGENDS

Figure 1. (A) A circle of a grid of 20x20 circles (with a radius of 100 μ m) placed over microscope slide. (B) Differential interference contrast micrograph of a sperm head. (C) Pseudocolor plot of the same spermatozoa.

375

Figure 2. High-power light microscope micrograph of sperm heads (1500X). (A) Crater-like appearance of nuclear vacuoles. (B,C,D) Spermatozoa with one or more vacuoles.

380

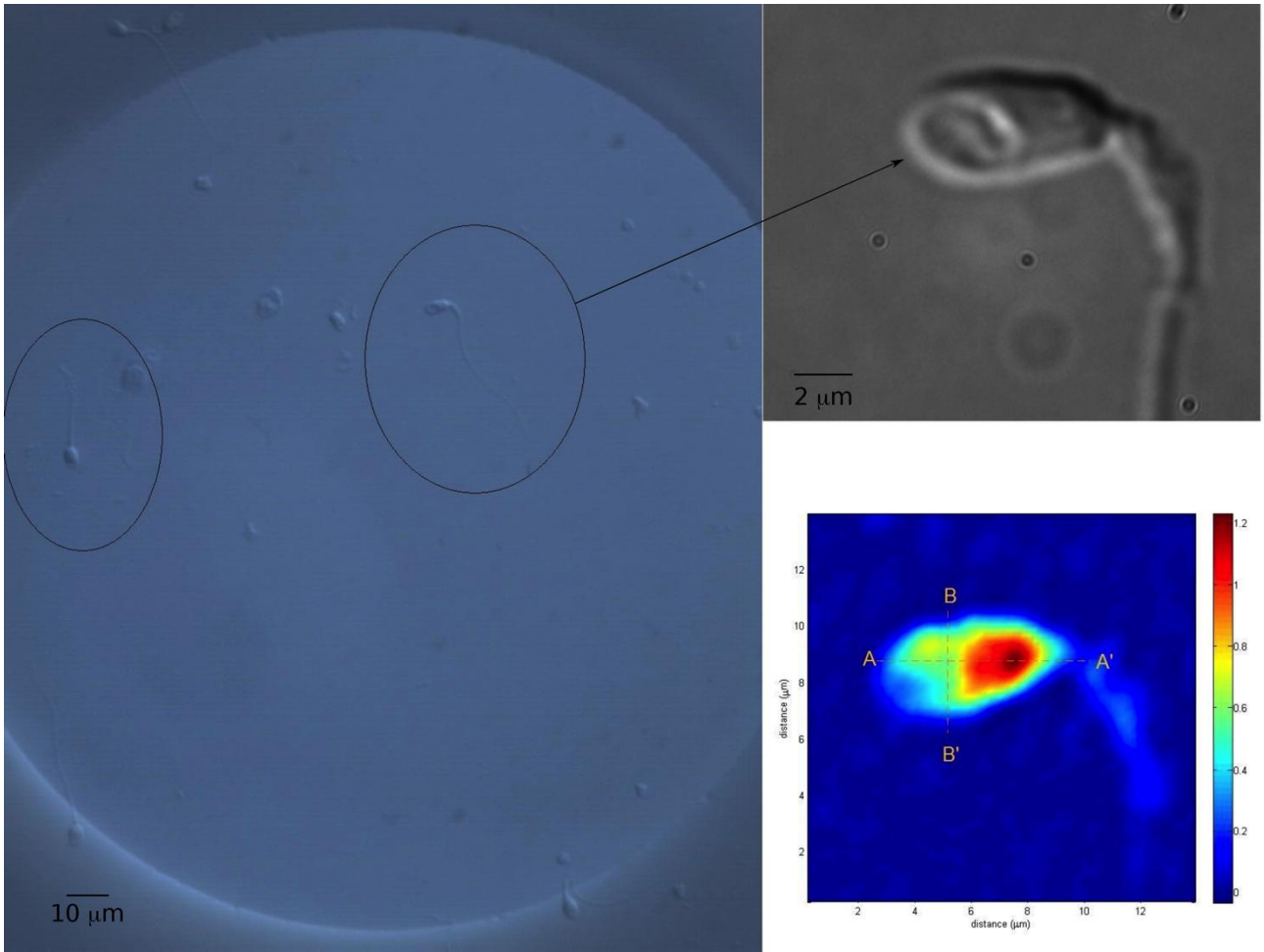
Figure 3. (a) Acquired hologram, a region is enhanced in order to show the interference pattern (inset). (b) Pseudocolor plot of a phase-contrast map for a human spermatozoon. (c) Pseudo 3-D representation of a human spermatozoon image reconstructed by DHM.

Figure 4. Profile plot along the lines (a) AA' and (b) BB', reported in Fig. 3(b).

385

Figure 5. Isolines plot of the reconstructed spermatozoon image.

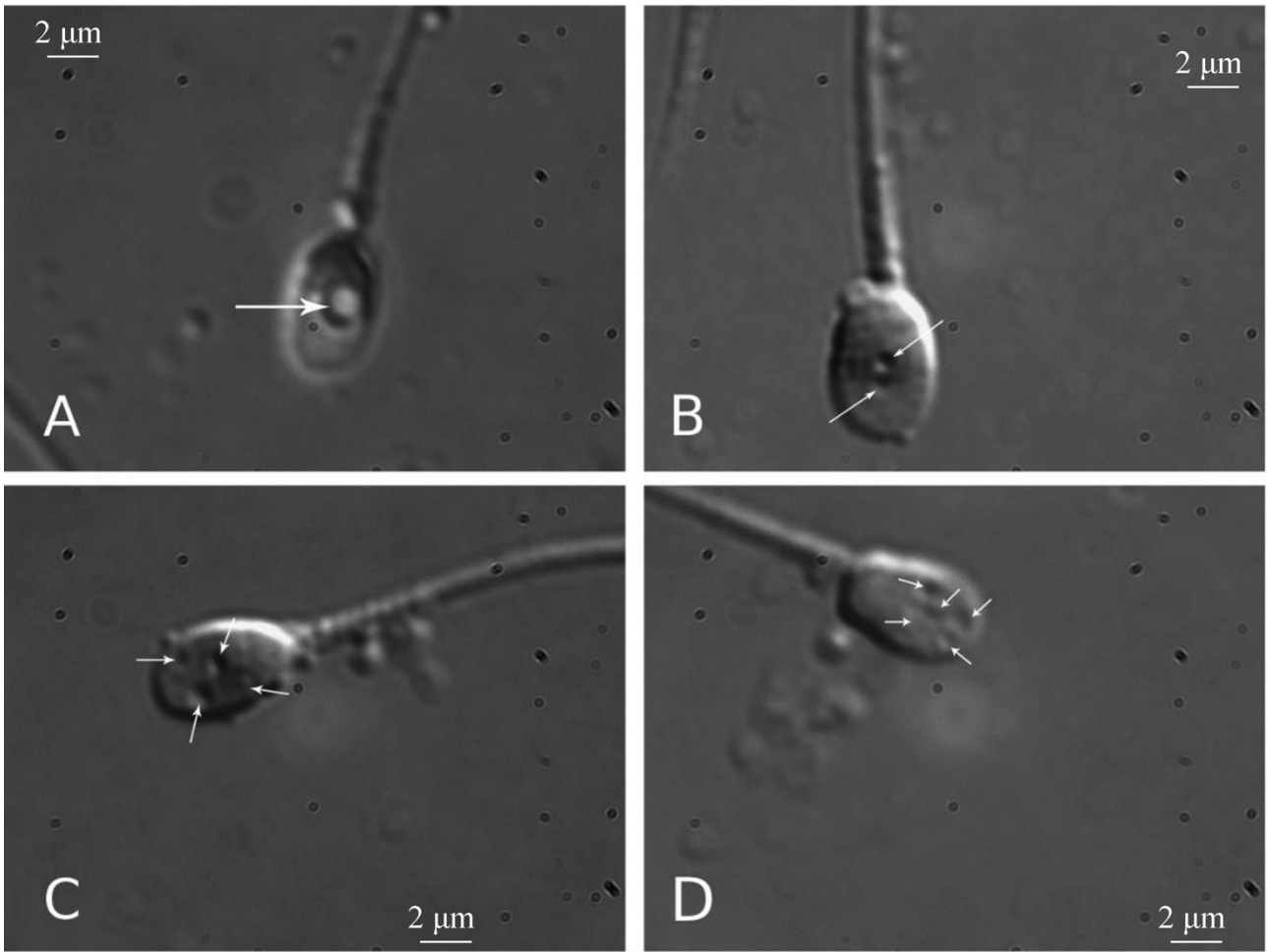
390 **Figure 6.** Comparison between a defect-free spermatozoa and a spermatozoa with vacuoles.



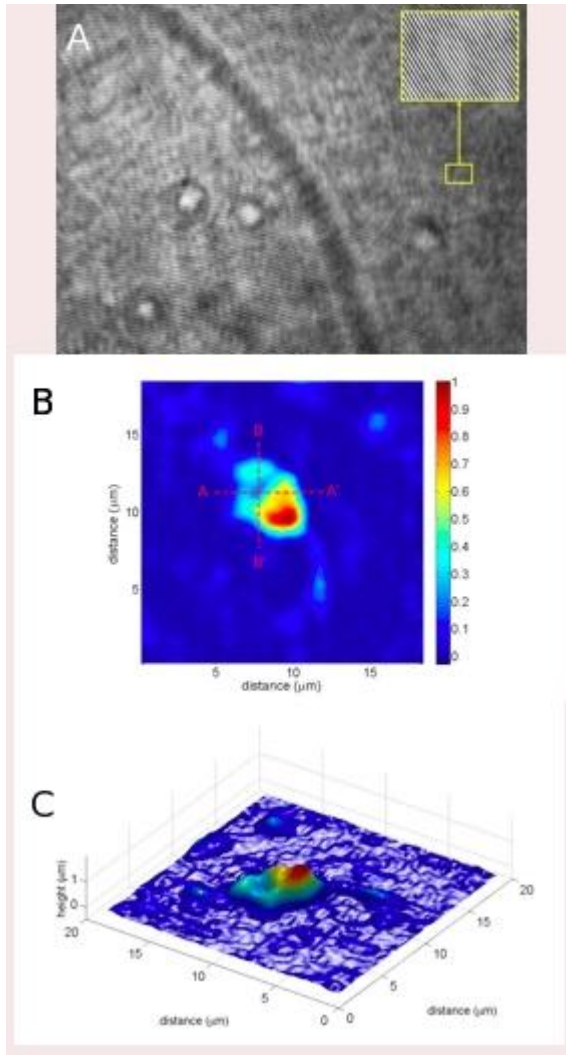
395

FIG. 1

400



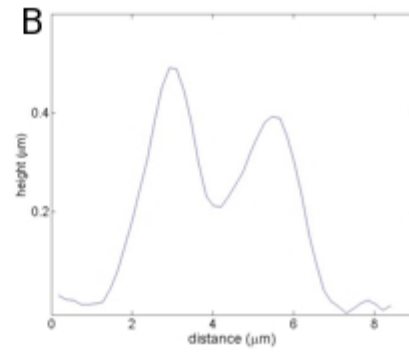
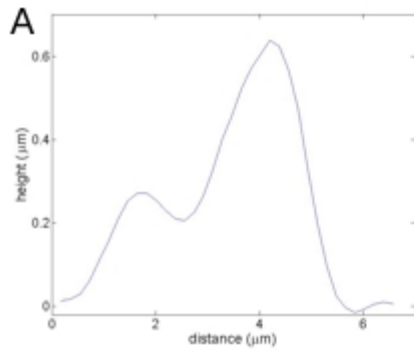
405 **FIG. 2**



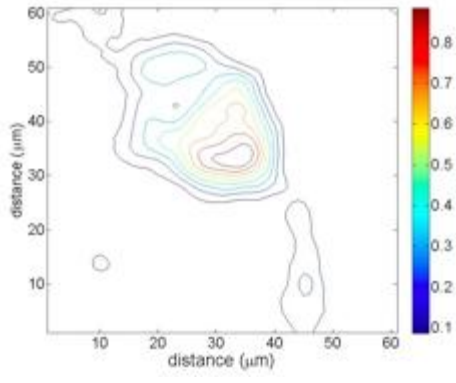
410

FIG. 3

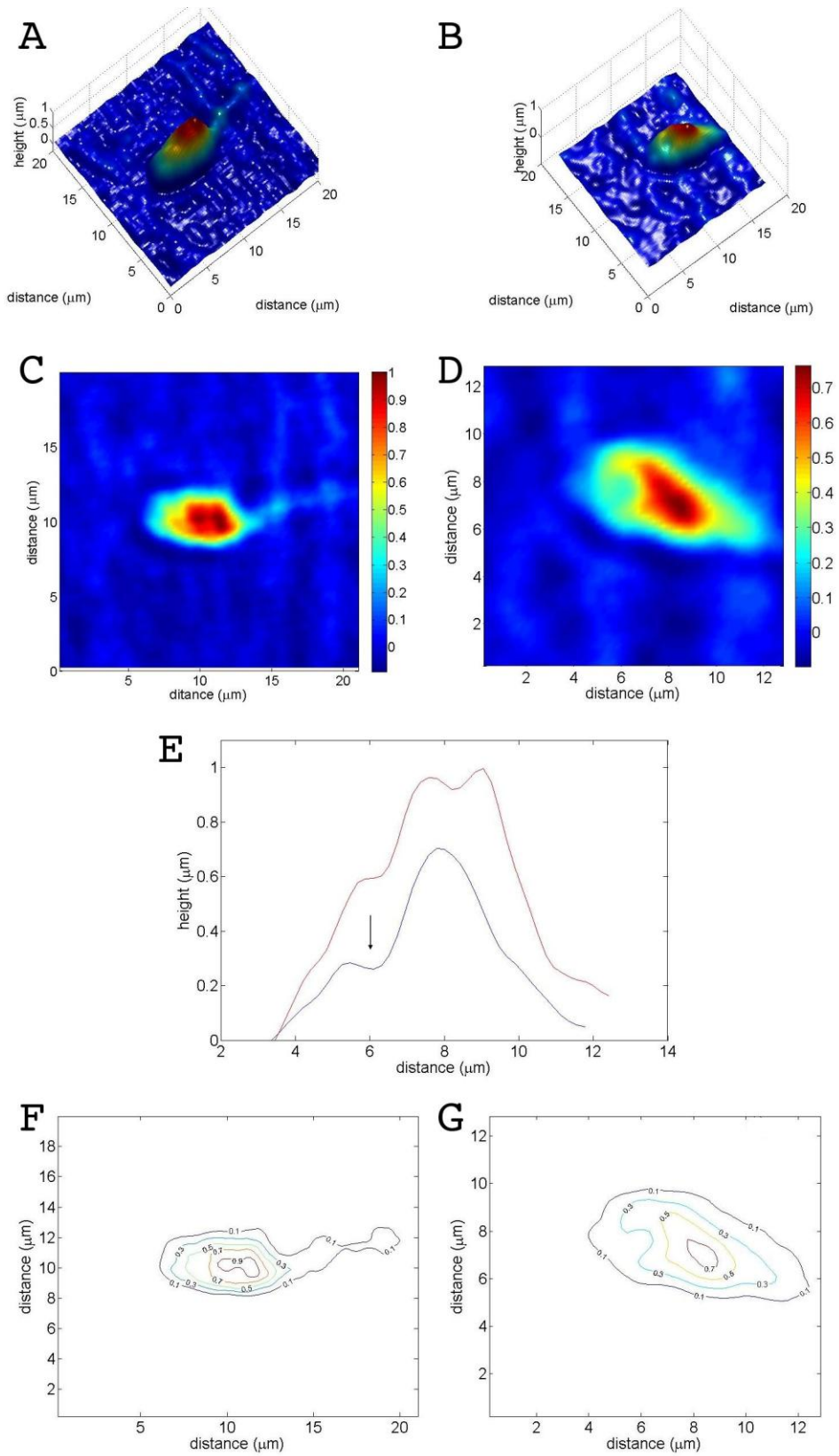
415



420 **FIG. 4**



425 **FIG. 5**



430

FIG. 6